JOURNAL OF MATERIALS SCIENCE 32 (1997) 1155–1161

An experimental study of the interaction of internal cracks in PMMA

Y. Z. LI, Y. T. CHOU
Department of Materials Science and Engineering, Lehigh University, Bethlehem, PA 18015, USA

Internal cracks in polymethyl methacrylate (PMMA) specimens were generated by pulsed laser light. The interactions of coplanar cracks, parallel cracks, and cracks in T and H configurations were investigated. The tensile strength of specimens with a single internal crack decreased with increasing crack size, and the strength correlated well with the initial crack and unstable crack size in the Griffith relationship. For specimens with coplanar and parallel cracks, the strength increased and decreased with the crack distance, respectively. For the T and H crack configurations, the presence of delamination cracks decreased the strength, and the reduction in strength became more significant when the crack distance was small. All fracture surfaces showed similar fracture morphology in the sequence of laser-generated crack, smooth fracture mirror, mist with hyperbolic markings, and rough hackle region with rib markings. Examination of the fracture surfaces revealed crack arrest by the delamination cracks in both T and H configurations, and crack bowing between delamination cracks in the H configuration. The propagating crack was eventually able to circumvent the delamination cracks. The experimental results are compared with the available theoretical analyses, and the relevance of the present study to the toughening of brittle materials is discussed.

1. Introduction

Inhomogeneities exist in materials. They are either inevitably introduced into the material system during fabrication or machining, or purposely added to strengthen the material, as with dislocations, inclusions, pores, large grains, microcracks, etc. Frequently, these inhomogeneities are the origin of material failure [1, 2]. Pre-existing microcracks or microcracks generated from other inhomogeneities, can either enhance or shield a macrocrack depending on their positions and orientations. On the one hand, microcracks can coalesce and grow into major cracks leading to final failure, especially in metallic materials [2, 3]. On the other hand, certain ceramic materials can be toughened through a microcracking process in which microcracks again play a key role [4–6].

Several analytical and numerical methods have been applied to analyse the interaction between two equal cracks [7], a microcrack and a macrocrack [8], among multiple microcracks [9, 10], as well as among microcracks and a macrocrack [11, 12]. Most analyses have dealt with two-dimensional cracks because of the mathematical complexity of three-dimensional problems. Some attempts to study the interaction of three-dimensional cracks with simple crack configurations have been made. O'Donoghue *et al.* [13] and Isida *et al.* [14] studied the interaction of far-spaced parallel elliptical cracks, while Fabrikant [15] and Kachanov and Laures [16] studied the interaction of closely spaced penny-shaped cracks. Laures and Kachanov [17] investigated the interaction of a macroscopic crack front with microcracks. However, in the experimental arena at large, very limited efforts have been made to study the three-dimensional crack interaction problems because of the difficulties in creating controllable internal cracks. Yoda [18] studied the growth and coalescence of two collinear indentation cracks. Choi and Salem [19] investigated the interaction of indentation cracks. Minchenkov *et al.* [20] studied the interaction between crack-like defects. In this paper, we report an experimental investigation of the interaction of internal three-dimensional cracks with typical configurations including coplanar, parallel, T, and H cracks. A brief report of the preliminary results for T and H crack configurations has been reported elsewhere [21].

2. Experimental procedure

Commercial PMMA sheets with a thickness of 12.7 mm and molecular weight of 2.6×10^6 (Acrylite GP supplied by Cyro Industries Company) were used in this study. Tensile specimens of dumb-bell shape were prepared with a cross-section of 11.0 mm × 12.7 mm and a length of 60 mm in the gauge section. The machining and subsequent polishing were made on the two saw-cut sides of the specimen, leaving the other two original surfaces intact for

TABLE I Specimen classification

	Crack configuration	No. of specimens used	No. of batches	No. of specimens in each batch
Group I	Coplanar cracks	35	7	5
Group II	Parallel cracks	30	6	5
Group III	Single crack	32	1	32
Group IV	T cracks	25	5	5
Group V	H cracks	5	1	5

laser irradiation. The planar initial cracks were generated by a focused ND:YAG pulsed laser beam with wavelength of 1064 nm. The detailed procedure for production of planar internal cracks in PMMA was described in an earlier work [22].

A total of 127 specimens were prepared and divided into five groups (see Table I). There were 35 specimens with internal coplanar cracks (group I), 30 with parallel cracks (group II), 32 with a single internal crack of varying size (group III), 25 with T cracks (group IV), and 5 with H cracks (group V), respectively (Fig. 1). Specimens in each group, except for group III, were further equally divided into batches, each with five specimens.

Owing to the scattering of crack size and fracture strength, specimens in each batch were prepared exactly in the same way to control the average crack size and the corresponding fracture strength. All cracks in specimens of the same group had the same nominal size, and cracks in Groups 4 and 5 specimens had the same size.

The crack size ($2a$) was determined before the fracture test and on the fracture surface after fracture by a Nikon microscope Optiphot with a drawing device (Nippon Kogaku K.K., Tokyo, Japan) together with a Micro-Plan II Image Analysis System PAD (Donsanto Corporation, Natick, MA). The average crack size for specimens in groups I, II, IV, and V was 0.87 ± 0.05, 0.90 ± 0.04, 0.90 ± 0.06, and 0.90 ± 0.06 mm, respectively (see Table II). The crack size of specimens in group III was in the range of 0.39–1.90 mm. The crack distance was measured between the crack centres for specimens in Groups I, II, and IV, and between the main crack and a delamination crack for Group V specimens (Table II).

Tensile testing was performed on an Instron 1350 system with a remote measurement system (Questar, New Hope, PA) to monitor the initiation and initial propagation of fracture. All specimens were tested at a loading rate of 12.7 mm min^{-1}. Fracture surfaces were examined using optical microscopy and scanning electron microscopy (Jeol 6300F).

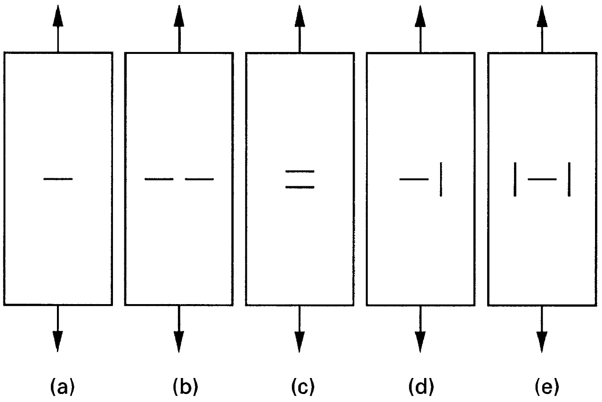

Figure 1 Crack configurations: (a) a single crack; (b) coplanar cracks; (c) parallel cracks; (d) T cracks; and (e) H cracks.

3. Results

A laser-generated internal crack in PMMA is shown in Fig. 2. It consists of three regions: a central damage region caused by direct absorption of laser energy, an intermediate cracking region, and a circumferential crazing region [22]. Most cracks so produced were not ideally circular, but were fairly close to elliptical shape with a ratio of the minor to major axis greater than 0.90 and in extreme cases as low as 0.75.

Fig. 3 shows the tensile strength as a function of crack distance for specimens with two coplanar cracks. Although the experimental data (○) have a large scattering, it is seen that the strength decreased with the crack distance, showing an enhancing effect of the crack interaction. The average crack size ($2a$) was 0.87 ± 0.05 mm. Numerical results ((●), see the

TABLE II The average crack size and distance

		Group I	Group II	Group IV	Group V
Crack size, $2a$ (mm)		0.87 ± 0.05	0.90 ± 0.04	0.90 ± 0.06	0.90 ± 0.06
Crack distance (mm)	Batch 1	0.90	0.15	0.45	0.80
	Batch 2	1.00	0.20	0.65	–
	Batch 3	1.15	0.25	0.80	–
	Batch 4	1.30	0.30	1.00	–
	Batch 5	1.50	0.40	Single crack	–
	Batch 6	2.00	Single crack	–	–
	Batch 7	Single crack	–	–	–

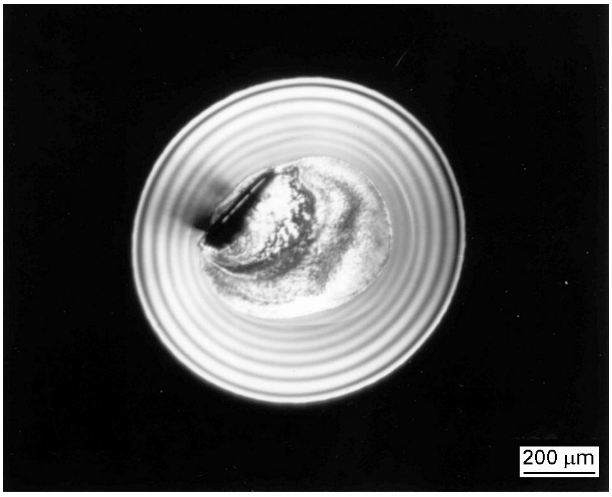

Figure 2 An internal crack generated by pulsed laser irradiation.

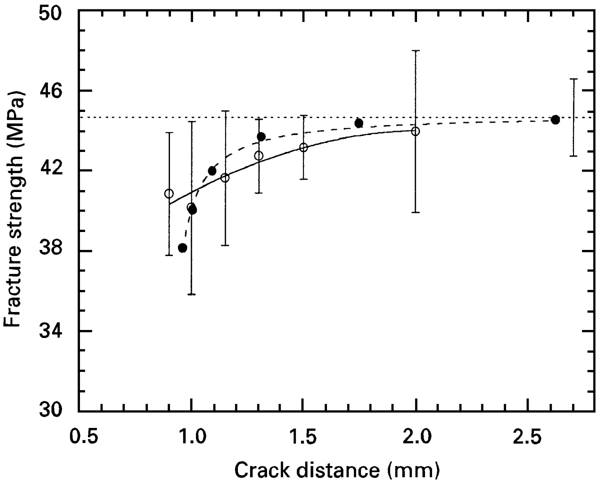

Figure 3 Fracture strength versus crack distance for the interaction of two coplanar cracks: (–○–) experimental, (–●–) theoretical and (- - -) single crack.

next section) show a strong dependence of strength on the crack distance for close interacting cracks.

For specimens with two parallel cracks, the average crack size was 0.90 ± 0.04 mm. The strength decreased with increasing crack distance (Fig. 4), showing a shielding effect of the interaction (○). This shielding effect is rather weak compared with the numerical results (●).

The effect of crack size on the specimen strength is shown in Fig. 5. As the crack size decreased from 1.90 mm to 0.39 mm, the specimen strength increased (○). The strength correlated well with the initial crack size and the size corresponding to the onset of unstable fracture in the Griffith relationship, $\sigma_f = 3.8 + Ca^{-1/2}$ with C being the slopes of the lines in Fig. 5. From fracture mechanics, $C = (\pi^{1/2}/2)\,K_{IC}$. The C values of 0.87 and 1.38 as measured from Fig. 5 give a K_{IC} value of 0.98 and 1.56 for the initial and unstable crack size, respectively. The constant 3.8 indicates a weak residual compressive stress field around the crack tip.

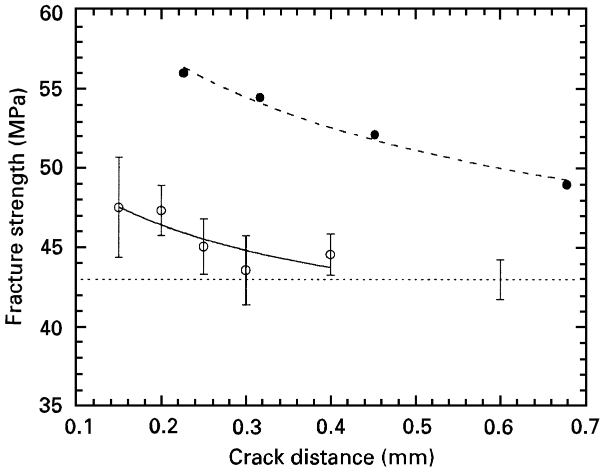

Figure 4 Fracture strength versus crack distance for the interaction of two parallel cracks. For key, see Fig. 3.

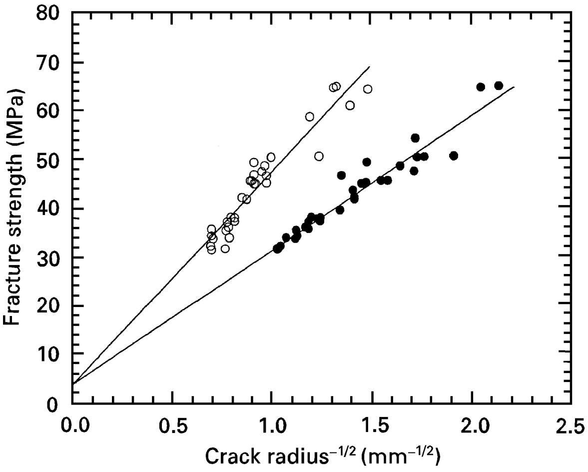

Figure 5 Relationship between fracture strength and crack size. (●) Initial crack size, (○) unstable crack size.

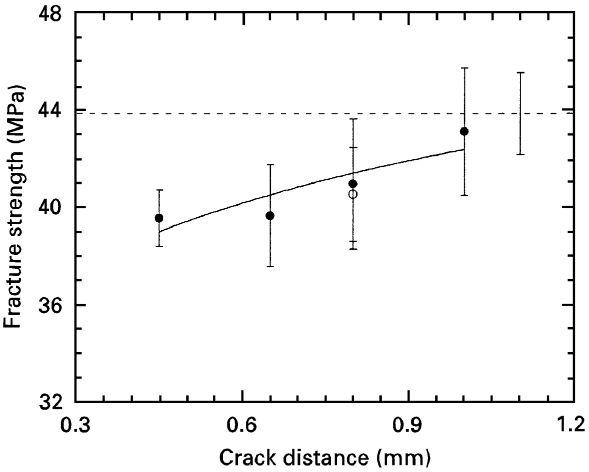

Figure 6 Fracture strength versus crack distance for the interaction of (–●–) T and (○) H cracks. (– – –) A single crack.

Fig. 6 shows that the presence of delamination cracks enhanced the stress intensity factor at the main crack, sitting normal to the loading direction. As a result, the specimen strength decreased with the crack distance, similar to the situation in the interaction of coplanar cracks. The strength of the specimens with H cracks was very close to that of those with T cracks for the same crack distance.

Fracture of all the specimens was initiated at the laser-generated internal crack, and the specimens broke into two halves with flat fracture surfaces. All fracture surfaces showed fracture morphology in the sequence of the laser-generated crack (the central elliptical region), a fracture mirror region caused by stable crack growth (the annular region between the inner ellipse and the outer circle), a mist region with hyperbolic markings, and a rough hackle region with rib markings (Fig. 7). Fig. 8 is a typical fracture surface of specimens with T cracks. At the top middle section, the dark region is the laser-damaged area. The intermediate grey region surrounding it was the initial crack. The annular brighter region covering the top half section is a fracture mirror. The horizontal dark band in the centre is the delamination crack. As can be seen in Fig. 8, the propagating crack front was arrested by, but was able to circumvent eventually, the delamination crack. Fig. 9 shows the tip region of the delamination crack. Interestingly, no river markings were visible down to this microscale. The fracture surfaces of specimens with H cracks show typical signs of crack bowing downward, while arrested at both sides by the delamination cracks (Fig. 10).

In most specimens, failure was not initiated simultaneously from the periphery of the crack as expected for an ideal penny-shaped crack or from the minor axis for an elliptical crack. As seen in Figs 7, 8, and 10, the fracture was not developed on a single plane. Instead, fracture was initiated at multiple sites. These propagating cracks were not lying exactly on the same plane, and when they met and overlapped, the fracture surface steps were formed, as seen in Figs 7, 8, and 10. The multiple initiations of fracture often lead to asymmetric fracture mirrors.

4. Discussion

A comparison is made below and discussed between the experimental results and available theoretical results for the interaction of coplanar and parallel cracks. The fracture behaviour of specimens with T and H cracks and their implications to the toughening of brittle materials will also be discussed.

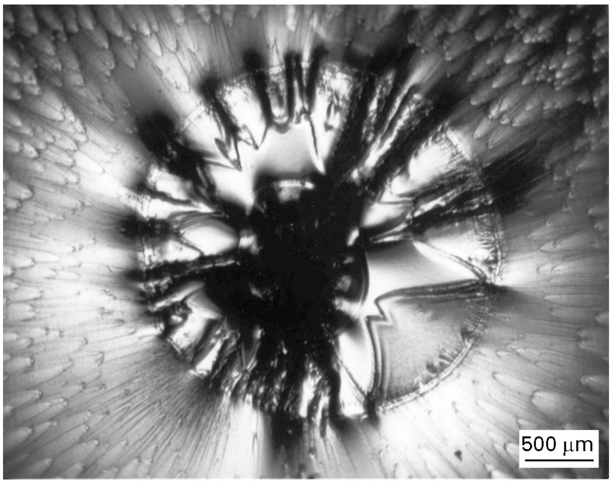

Figure 7 Fracture surface of specimen with a single crack showing typical sequential features (from centre to radial direction): laser-generated crack, fracture mirror, and mist with hyperbolic markings.

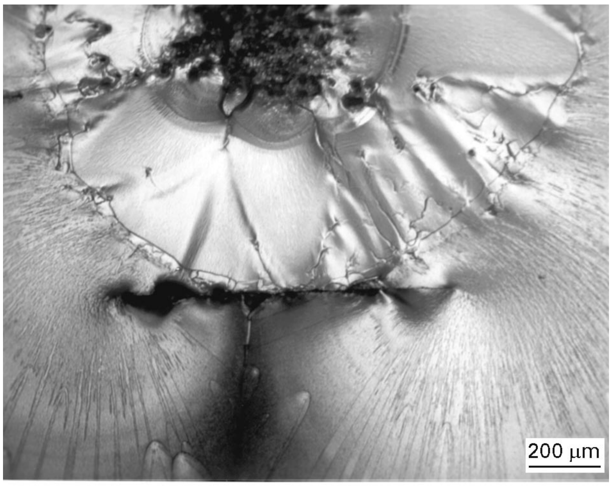

Figure 8 Typical fracture surface of specimen with T cracks showing crack arrest by the delamination crack in the centre of the picture.

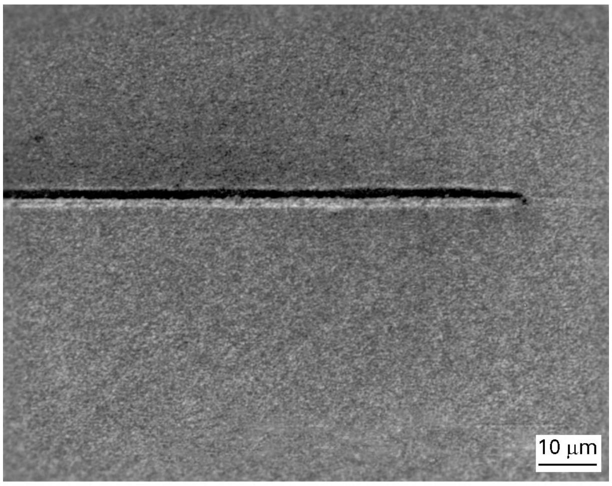

Figure 9 Scanning electron micrograph showing the tip of the delamination crack in Fig. 8.

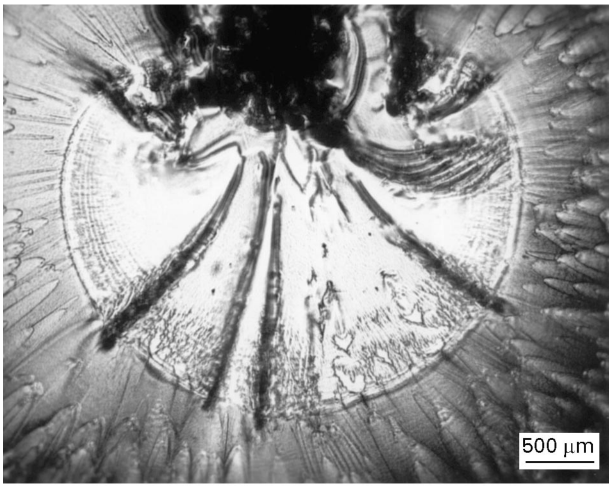

Figure 10 Photomicrograph for H crack configuration showing crack bowing downwards when arrested by delamination cracks at both sides.

4.1. Simplification of crack shape

Most cracks were not exactly penny-shaped. Each crack on the fracture surface approximated an elliptical shape with a major and a minor axis. For most cracks measured, the ratio of minor to major axis is greater than 0.85, with no cracks having a ratio less than 0.75.

The model I stress intensity factor, K_I, for an embedded elliptical crack with major axis a and minor axis c (Fig. 11) is [23]

$$K_I = \frac{\sigma(\pi c)^{1/2}}{\Phi}\left(\sin^2\varphi + \frac{c^2}{a^2}\cos^2\varphi\right)^{1/2} \tag{1}$$

where φ is the angle from the major axis and Φ is the elliptic integral of the second kind, given by

$$\Phi = \int_0^{\pi/2}\left(1 - \frac{a^2 - c^2}{a^2}\sin^2\varphi\right)^{1/2} d\varphi \tag{2}$$

The maximum and minimum stress intensity factors, $(K_I)_{max}$ and $(K_I)_{min}$, occur at points A and B, respectively. If $K_I(a) = (2/\pi^{1/2})\,\sigma(\pi a)^{1/2}$ and $K_I(c) = (2/\pi^{1/2})\,\sigma(\pi c)^{1/2}$ are the stress intensity factors for an embedded penny-shaped crack with radius a, and c, respectively, then, $(K_I)_{min} < K_I(c) < (K_I)_{max} < K_I(a)$. The maximum stress intensity factor for the elliptical crack becomes

$$(K_I)_{max} = \frac{\sigma(\pi c)^{1/2}}{\Phi} = C(a,c)\,K_I(a) \tag{3}$$

with

$$\begin{aligned} C(a,c) &= \frac{\pi(c/a)^{1/2}}{2\Phi} \\ &= 0.991 \\ &\approx 1.000 \qquad \text{for } c/a \geqslant 0.80 \end{aligned} \tag{4}$$

The coefficient $C(a,c)$ is given in Table III for the different c/a ratios. For $c/a = 0.80$, the difference between $K_I(a)$ and $(K_I)_{max}$ is less than 1%. Therefore, as a rough approximation, the elliptical crack can be treated as a penny-shaped crack with a radius of the corresponding elliptical major axis for the purpose of evaluation of the maximum stress intensity factor or fracture strength.

4.2. Theoretical results for the interaction of coplanar and parallel cracks

Kachanov and Laures [16] evaluated the interaction of internal coplanar and parallel penny-shaped cracks of equal size under mode I loading. For a given crack distance, the stress intensity factor in terms of that for a single crack, K_I/K_{I0}, is given in Table 2 of [16] for coplanar cracks, in Table 5 of [16] for parallel cracks. Poisson's ratio, ν, was taken as 0.25 in their calculations. The numerical results of the specimen strength with interacting cracks can be calculated from $\sigma_f = \sigma_0/(K_I/K_{I0})$, where σ_0 is the average strength of specimens with a single crack ((●) in Figs 3 and 4).

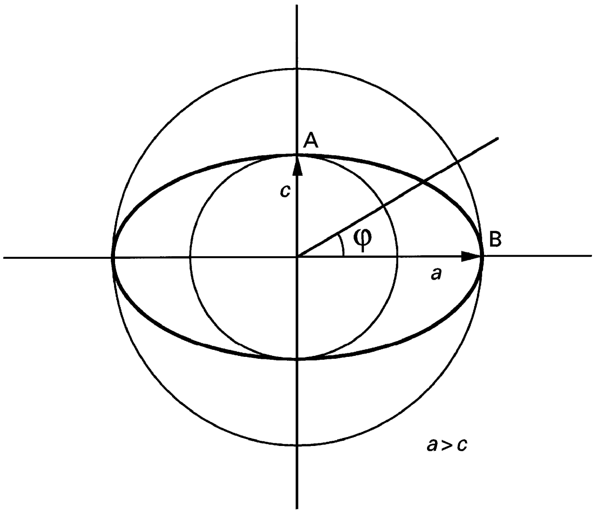

Figure 11 Schematic drawing of an elliptical crack and two circular cracks with radii being the major and minor axes of the elliptical crack, respectively.

TABLE III Maximum stress intensity factor of an elliptical crack with major axis a and minor axis c in terms of the stress intensity factor of a penny-shaped crack with a radius of the major elliptical axis

	c/a values				
	0.95	0.90	0.85	0.80	0.75
$(K_I)_{max}$	0.9995 $K_I(a)$	0.9979 $K_I(a)$	0.9951 $K_I(a)$	0.9907 $K_I(a)$	0.9847 $K_I(a)$

4.3. Comparison between the experimental and theoretical results

As shown in Fig. 3, the strength of specimens with coplanar cracks decreased as the crack distance decreased. When the distance between the crack centres was about twice the crack diameter, the specimen strength approached that of specimens with a single crack. This means that the interaction between the two coplanar cracks would be very weak when the cracks are apart to that extent. The theoretical result shows the same trend as the experimental result but with stronger dependence on crack distance for close cracks. However, the large experimental error makes more accurate comparison less meaningful.

For specimens with parallel cracks, the experimental and theoretical results also show the same trend, but with the former much weaker than the latter (Fig. 4). Such a difference may result from two possible reasons. First, the theoretical analysis considered an ideal elastic material. When two cracks are very closely stacked, the material between the cracks would yield and give less shielding than that predicted by the elastic analysis. Secondly, when two parallel cracks are close, a residual tensile stress would exist at the crack tip so that only a small load is needed to fracture the specimen. More accurate experimental work is needed to evaluate critically the crack interaction.

4.4. Fracture initiation and crack stability

The fracture strength correlated well with the initial crack size and the fracture mirror size in the Griffith relationship (Fig. 5), and led to a K_{IC} value of 0.98 and 1.56 MPa m$^{1/2}$, respectively. In the load–displacement chart and the remote measurement system, the fracture process seemed catastrophic. No stable growth nor load change after the fracture initiation was recorded. If both the fracture initiation stress and the stress at the unstable crack size are taken as the fracture strength, then the present result is in close agreement with the work of Marshall *et al.* [24]. The latter measured a K_{IC} value of 0.9 MPa m$^{1/2}$ for fracture initiation and 1.6 MPa m$^{1/2}$ for onset of unstable growth at the loading rate of 1.27 cm min^{-1}.

The residual stress field around the crack tip indicated by Fig. 5 qualitatively represents the situation of the laser-generated internal cracks. The absorption of the laser energy causes local material melting and crack generation which releases most of the thermal stresses. As the matrix cools down, the mismatch between the volume contraction of the damage zone and that of the matrix results in a residual stress field in the vicinity of the crack tip. Because of the rather small temperature difference and the viscoelastic behaviour of PMMA, the residual stress field is relatively weak. Interestingly, in the case of fused quartz, the residual stress field is tensile, as indicated by the experimental plot of the strength versus crack size [25]. Because of the scattering of data, more accurate and quantitative measurement is needed to understand fully the residual stress field.

4.5. Implication for the toughening of brittle matrices

Sakai *et al.* [26] modelled the interaction of a two-dimensional crack and a delamination crack using the finite element method. These authors predicted an enhanced fracture initiation by the main crack, which was later completely arrested by the delamination crack when a stable T-shaped crack was formed. They were able experimentally to achieve a fracture toughness normal to the interlaminar plane 15 times higher than that along the interlaminar plane for a laminate pyrolytic carbon material.

The fact that specimens with both H and T crack configurations had very close strength values (Fig. 6) suggests that the delamination cracks significantly affect only the stress distribution of the crack tip close to the delamination crack. Our observation of strength reduction for T cracks clearly showed an enhanced fracture initiation, in qualitative agreement with the results of Sakai *et al.* [26].

However, as shown in Figs 8 and 10, the three-dimensional crack kept growing in radial directions after a portion of its front was arrested, and was eventually able to circumvent the delamination cracks and to fracture. This suggests that a crack normal to the layers in laminated structures can still grow along the barrier after being arrested. When the crack propagated to both end surfaces of the material, the crack might have acquired enough dynamic energy to cut through the shielding layer interfaces and lead to final fracture. Therefore, the widely used notched three- or four-point bending test and single-edge notched beam test of laminated materials may overestimate the effectiveness of toughening, because the evaluations are based on completely arrested (large) initial notch cracks. The effectiveness of lamination toughening can be improved by optimizing the laminate thickness for a given service load to avoid the premature initiation of fracture by small cracks.

As seen in Figs 8 and 10, the main crack was able to circumvent the delamination cracks when a portion of its front was arrested by the latter. Such a circumvention process indicates the possible existence of a sliding and pull-out toughening mechanism by second-phase platelet particles with weak interfaces between the matrix and the platelets. The increase in toughness has been experimentally observed in corundum–rutile composites [27] and silicon carbide platelet-reinforced alumina [28]. Because the bridging platelets in the crack interface behind the main crack tip have more frictional areas than fibres, and require more frictional energy for pull-out, platelets may be thus more effective in toughening brittle matrices than the current widely used reinforcement by fibres/whiskers. Also, platelet-reinforced matrices would have more isotropic mechanical properties. Because the weak interfaces between platelets and matrix reduce the material strength, the size of the platelets needs to be optimized for favourable strength and toughness.

The arrest of crack growth by delamination cracks and crack bowing between the H cracks suggest another, though less effective, toughening mechanism predicted by Lange [29], Evans [30], and Green [31] in second-phase-reinforced brittle matrices with weak interfaces between the reinforcing elements and the matrix. On the other hand, the material strength may be reduced by the presence of such weak interfaces (Fig. 6). The strength and toughness can be optimized by choosing an appropriate size and volume ratio for the reinforcing elements.

5. Conclusions

The interactions of internal coplanar, parallel, T-, and H-shaped cracks were investigated experimentally. The results can be summarized as follows.

1. The strength of specimens with coplanar cracks of equal size decreased with the crack distance, but more gradually as compared with the theoretical result.

2. The strength of specimens with equal parallel cracks decreased with increasing crack distance, and the interaction was weaker than that predicted by the theoretical analysis.

3. The presence of delamination cracks decreased the material strength, and the reduction became more significant when the main and delamination cracks were close.

4. The fracture strength correlated well with the initial crack size and the size of the onset of unstable

fracture in the Griffith relationship, confirming that there is an initial stable crack growth before catastrophic fracture.

5. Examination of the fracture surfaces suggests that it is possible to achieve more effective toughening of brittle matrices by adding second-phase platelets.

Acknowledgement

This work was supported by the US Army Research Office through grant DAAL 03-91-G-0077.

References

1. G. D. QUINN, *J. Am. Ceram. Soc.* **74** (1991) 2307.
2. D. BROEK "Elementary Engineering Fracture Mechanics" (Martinus Nijhoff, The Hague, 1982) Ch. 2.
3. R. N. PARKINS and P. M. SINGH, *Corrosion* **46** (1990) 485.
4. A. G. EVANS, *Scripta Metall.* **10** (1976) 93.
5. J. W. HUTCHINSON, *Acta. Metall.* **35** (1987) 1605.
6. H. CAI and K. T. FABER, *J. Appl. Mech.* **59** (1992) 497.
7. V. G. UKADGAONKER and A. P. NAIK, *Int. J. Fract.* **51** (1991) 219.
8. S. X. GONG, *ibid.* **66** (1994) R51.
9. K. Y. LAM and S. P. PHUA, *Eng. Fract. Mech.* **40** (1991) 585.
10. D. A. LOCKNER and T. R. MADDEN, *J. Geophys. Res.* **96B** (1991) 9623.
11. M. KACHANOV and E. MONTAGUT, *Eng. Fract. Mech.* **25** (1986) 625.
12. S.-X. GONG and H. HORRI, *J. Mech. Phys. Solids* **37** (1989) 27.
13. P. E. O'DONOGHUE, T. NIOSHIKA and S. N. ATLURI, *Int. J. Numer. Meth. Eng.* **21** (1985) 437.
14. M. ISIDA, K. HIROTA, H. NOGUCHI and T. YOSHIDA, *Int. J. Fract.* **27** (1985) 31.
15. V. I. FABRIKANT, *Acta Mech.* **67** (1987) 39.
16. M. KACHANOV and J.-P. LAURES, *Int. J. Fract.* **41** (1989) 289.
17. J.-P. LAURES and M. KACHANOV, *ibid.* **48** (1991) 255.
18. M. YODA, *Int. J. Fatigue* **11** (1989) 429.
19. S. R. CHOI and J. A. SALEM, *J. Mater. Sci.* **28** (1993) 501.
20. O. S. MINCHENKOV, N. A. KOSTENKO and Y. I. POPOV, *Strength Mater.* **22** (1991) 973.
21. Y. Z. LI and Y. T. CHOU, *J. Mater. Sci. Lett.* **15** (1996) 219.
22. Y. Z. LI and Y. T. CHOU, *Mater. Sci. Eng.* **A194** (1995) 113.
23. G. R. IRWIN, *Trans. ASME, Ser. E. 85 J. Appl. Mech.* **29** (1962) 651.
24. G. P. MARSHALL, L. H. COUTTS and J. G. WILLIAMS, *J. Mater. Sci.* **9** (1974) 1409.
25. Y. Z. LI, M. P. HARMER and Y. T. CHOU, *J. Mater. Res.* **9** (1994) 1780.
26. M. SAKAI, S. TAKEUCHI, D. B. FISCHBACH and R. C. BRADT, in "Ceramic Microstructures: Role of Interfaces", edited by J. A. Pask and A. G. Evans (Plenum, New York, 1987) p. 869.
27. S. HORI, H. KAJI, M. YOSHIMURA and S. SŌMIYA, in "Advanced Structural Ceramics", Vol. 78, edited by P. F. Becher, M. V. Swain and S. Sōmiya (Materials Research Society, Pittsburgh, PA, 1987) p. 283.
28. K. B. ALEXANDER, P. F. BECHER and S. B. WATERS, in "Proceedings of the 12th International Congress for Electron Microscopy", edited by L. D. Peachey and D. B. Williams (San Francisco Press, San Francisco, CA, 1990) p. 1032.
29. F. F. LANGE, *Philos. Mag.* **22** (1970) 983.
30. A. G. EVANS, *ibid.* **26** (1972) 1327.
31. D. J. GREEN, *J. Am. Ceram. Soc.* **66** (1983) C4.

Received 23 February
and accepted 31 July 1996